The H+*para*-H_2 reaction: Influence of dynamical resonances on H_2 ($v'=1$, $j'=1$ and 3) integral cross sections

Dahv A. V. Kliner, David E. Adelman, and Richard N. Zare
Department of Chemistry, Stanford University, Stanford, California 94305

(Received 17 August 1990; accepted 5 October 1990)

We have measured integral rate constants for the reaction $H + para\text{-}H_2 \rightarrow H_2(v' = 1, j' = 1$ and $3) + H$ at 11 center-of-mass collision energies (E_{rel}) between 0.88 and 1.01 eV, a region in which dynamical scattering resonances are present. We have also measured the $H_2(v' = 1, j' = 3)/H_2(v' = 1, j' = 1)$ population ratio at two additional values of E_{rel} outside of this range. Tunable uv laser photolysis of HI was used to generate translationally hot H atoms of variable kinetic energy. Quantum-state-specific detection of the H_2 reaction product was accomplished via $(2+1)$ resonance-enhanced multiphoton ionization and time-of-flight mass spectrometry. The integral rate constants have a smooth dependence on E_{rel}, in agreement with the recent quantum-mechanical (QM) calculations of Zhang and Miller and contrary to the experimental results of Nieh and Valentini. The QM results are in nearly perfect agreement with the present measurements for the dependence on E_{rel} of both the integral rate constants and the $H_2(v' = 1, j' = 3)/H_2(v' = 1, j' = 1)$ population ratio. It is concluded that measurements of integral cross sections as a function of collision energy are not highly sensitive to the presence of dynamical resonances in this system.

I. INTRODUCTION

Dynamical scattering (Feshbach) resonances are one of the most intriguing quantum-mechanical (QM) effects in bimolecular chemical reactions.[1–3] Such a resonance refers to a metastable collision complex that is formed when reagents collide with the appropriate energy to excite a vibration of the complex. The excited complex subsequently decays either to reactants or to products. The outcome of the scattering event can be significantly influenced by accessing the resonance state. Interference between resonant and direct scattering waves produces oscillations in the reaction probability. Thus, in QM scattering calculations, resonances are associated with increases in reaction times in comparison with direct reactions, and they appear as sharp variations in differential reaction cross sections as a function of collision energy.

The collision energies at which resonances occur correspond to the eigenenergies of the quasibound complex. The widths are determined by the lifetimes of these states. Thus, the energies and widths of resonances are sensitive to the topology of the potential energy surface (PES) in the region of the saddle point. The identification of dynamical scattering resonances is a "spectroscopy of the transition state" of a bimolecular chemical reaction. This has generated intense interest in their detection and characterization as a sensitive test of PESs and of reactive scattering calculations performed on them.[4]

Resonances in reactive scattering first appeared in one-dimensional (collinear) QM calculations of the $H + H_2$ reaction by Kuppermann and co-workers[5] and by Wu and Levine.[6] They were later found in the three-dimensional QM $H + H_2$ calculations of Schatz and Kuppermann[7] for the $J = 0$ and $J = 1$ partial scattering waves, where J is the total angular momentum. An important question was whether the resonance structure would be "washed out" by the summation over J required to calculate the fully converged, integral reaction cross sections. Early work indicated that the structure would survive this summation,[7] but more recent work has suggested that it would not.[3,8]

While most theoretical studies of dynamical resonances have been concerned with the $H + H_2$ reaction, most experimental measurements have been performed on other systems. The first experimental evidence that resonances influence a measurable quantity in a bimolecular chemical reaction was provided by Lee and co-workers[4] for the $F + H_2$ system (and its isotopic variants). These workers measured angular and time-of-flight (TOF) distributions of the HF product in a crossed-beam apparatus at several center-of-mass collision energies (E_{rel}). The angular distributions were dominated by backward scattering for most product vibrational levels, but were both forward and backward scattered for certain vibrational states. This behavior was attributed to the presence of dynamical resonances. This interpretation remains controversial,[3] partly because of the lack of an adequate HHF PES.[9] While it is possible to access resonances via photodetachment of the stable, anionic analogs of the transition states of bimolecular reactions,[10] no such measurement is presently available for H_3.

In the past two years, the results of fully converged, three-dimensional, QM calculations performed on accurate, *ab initio* PESs have become available for members of the $H + H_2$ reaction family.[11–19] Parallel developments in experimental methodologies have provided measurements that can be compared with these benchmark theoretical calculations.[20–27] The issue of the influence of dynamical scattering resonances on $H + H_2$ integral cross sections can now be addressed by both theory and experiment.

Most experiments performed on the $H + H_2$ reaction

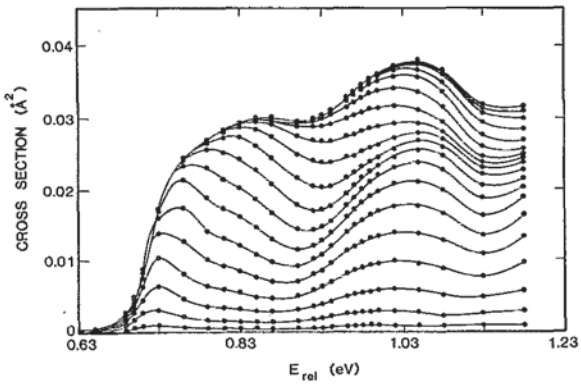

FIG. 1. Integral cross section for the reaction $H + H_2(v=0, j=0) \rightarrow H_2(v'=1, j'=1) + H$ as a function of collision energy, adapted from Fig. 2 of Ref. 12. The various curves connecting the calculated points are for the various values of J_{max}, the upper limit in the sum over total angular momentum in the QM calculation. The lowest curve is $J_{max} = 0$, the next $J_{max} = 1$, and the uppermost $J_{max} = 18$.

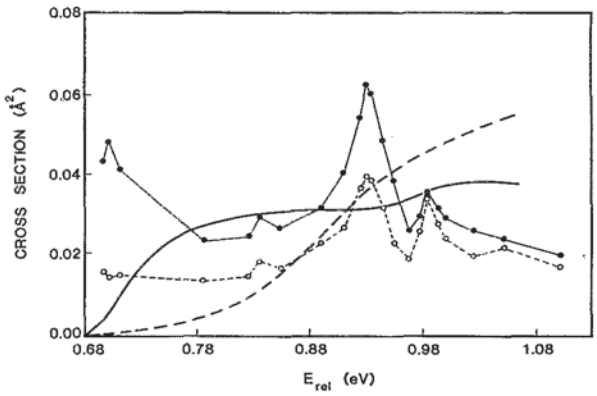

FIG. 2. Integral cross sections for the reaction $H + p\text{-}H_2 \rightarrow H_2(v'=1, j') + H$ as a function of collision energy for $j'=1$ (solid circles and solid curves) and $j'=3$ (open circles and dashed curves), adapted from Fig. 4 of Ref. 12. The points connected by lines are the experimental results of NV; the smooth curves are the QM results of ZM.

family have used isotopic substitution to distinguish reactants from products, i.e., have investigated the $H + D_2$ or $D + H_2$ reactions.[27] In contrast, all of the early QM calculations, as well as many recent ones, were for the nonisotopically labeled variant. The unlabeled reaction can be made accessible experimentally by taking advantage of the existence of two nuclear-spin states of H_2, *para*-H_2 (p-H_2, $J = 0,2,4,\cdots$) and *ortho*-H_2 (o-H_2, $J = 1,3,5,\cdots$).[28] Inelastic collisions cannot interconvert p-H_2 and o-H_2, while reactive collisions can. Hence, the $H + H_2$ reactive scattering channel can be isolated for study by using p-H_2 as a reagent and by monitoring the o-H_2 product.

Nieh and Valentini[21] (NV) reported the first experimental evidence that effects of dynamical resonances are observable in integral cross sections for the reaction $H + p\text{-}H_2 \rightarrow H_2(v', j') + H$ (these experiments actually measured rate constants rather than cross sections,[29] though the distinction is not important for the present purposes). Coherent anti-Stokes Raman spectroscopy (CARS) was used to measure the $H_2(v', j')$ integral cross sections for $E_{rel} = 0.69$–1.10 eV. NV observed sharp variations in the $v' = 1$ cross sections for the formation of o-H_2 and p-H_2 as the collision energy was varied. The peaks were assigned to qausibound, excited states of the H_3 complex containing one quantum of symmetric stretch and either zero or two quanta of bending excitation. Similar structure is not present in the integral cross sections obtained from the fully converged QM calculations of Zhang and Miller[12] (ZM). While resonance structure is found for individual partial scattering waves, the averaging over partial waves diminishes the influence of the resonances so that only weak undulations remain in the integral cross sections. This blurring of the resonance structure is shown in Fig. 1. Figure 2 presents a comparison between the $H + p\text{-}H_2 \rightarrow o\text{-}H_2(v'=1, j'=1 \text{ and } 3) + H$ integral cross sections derived from the measurements of NV and from the calculations of ZM. This comparison has resulted in the most significant disagreement between QM theory and experiment for the $H + H_2$ reaction family.[19]

The $H_2(v'=1, j')$ product rotational distributions reported by NV are also in disagreement with those determined by ZM. In particular, at all collision energies NV measured the $H_2(v'=1, j'=3)/H_2(v'=1, j'=1)$ population ratio to be less than unity; the ratio obtained from the QM computations is less than unity at low energies and greater than unity at higher energies.

Phillips, Levene, and Valentini[22] reported further experimental evidence of the influence of dynamical resonances for a member of the $H + H_2$ reaction family. These workers again used CARS to measure internal state distributions of the $HD(v', j')$ product of the $D + H_2$ reaction at two values of E_{rel}, 0.67 and 0.79 eV. They found enhanced vibrational excitation at the lower energy, attributing this enhancement to the presence of a resonance. Although this resonance appears in the lowest partial waves in the QM calculations of Zhang and Miller[15] and of Zhao *et al.*,[18] it disappears in the sum over partial waves.

Several papers have appeared attempting to resolve these discrepancies. The $H + p\text{-}H_2$ results of ZM were reproduced by Manolopolous and Wyatt[13] and by Launay and Le Dourneuf,[14] indicating that the QM calculations were probably correct for the given PES. NV suggested that the lack of resonances in these QM calculations could arise from errors in the LSTH[30] PES on which the computations were performed. However, later QM calculations by Manolopoulos and Wyatt[16] using the newer DMBE[31] surface were in close accord with the earlier results. Similarly, QM calculations of integral cross sections for the $D + H_2$ reaction performed on the LSTH PES[15] and on the DMBE PES[18] are in close agreement. Bauschlicher, Langhoff, and Partridge[32] calculated additional *ab initio* energies for the H_3 PES, with emphasis on bent geometries. These workers found that both the LSTH and DMBE surfaces agree well with their calculations, with the DMBE surface providing a somewhat better fit to the new *ab initio* points. Bauschlicher *et al.*[32] concluded that these new calculations confirmed that the differences between theory

and experiment were not the result of errors in the *ab initio* surface, in agreement with the conjecture of Zhang and Miller.[33]

Two theoretical groups calculated quantities that involve less averaging than integral cross sections in an attempt to obtain structure similar to that of NV. Zhang and Miller[33] calculated $H_2(v', j')$ differential (angle resolved) cross sections as a function of E_{rel}. These cross sections show structure similar to that of individual partial scattering waves, but still not as pronounced as that reported by NV. Manolopoulos and Wyatt[13] noted that their calculated $H + p\text{-}H_2 \rightarrow H_2(v' = 1, j' = 0) + H$ differential cross sections, which contain both inelastic and reactive contributions, exhibit more resonance structure than the purely reactive cross sections.

Muga and Levine[34] proposed a classical mechanism for resonances in the $H + p\text{-}H_2$ reaction in which high impact parameter (high J) trajectories are deflected toward a collinear H_3 configuration by the long-range barrier to insertion. However, the features of the PES and range of J values that contribute to this mechanism are included in the converged QM calculations.[19]

Krause and Shapiro[35] postulated that high-intensity CARS laser beams could optically probe the H_3 transition state, with an enhancement in the signal being observed as E_{rel} is scanned through a scattering resonance. This enhancement arises from the relatively long lifetime of the H_3 transient at this energy. Recently, Seideman, Krause, and Shapiro[36] suggested a refinement in which laser catalysis of the reaction could cause the sharp features observed by NV. These hypotheses were based on one-dimensional (collinear) $H + H_2$ QM calculations.

Both the present experiment and that of NV were performed under "bulb" conditions. A calculation of the collision-energy spread in such experiments was recently performed by van der Zande, Zhang, and Zare.[37] Their analysis shows that the E_{rel} distribution for $H + H_2$ is nearly Gaussian with a FWHM of 0.3 eV. The sharp features observed by NV (Fig. 2) appear to be narrower than the experimental energy resolution. Van der Zande *et al.*[37] concluded that a reinterpretation of the experimental results was required.

In this paper we report new measurements, comparable to those of NV, for the reaction $H + p\text{-}H_2 \rightarrow o\text{-}H_2(v' = 1, j') + H$. We used $(2+1)$ resonance-enhanced multiphoton ionization (REMPI) to measure the relative rate constants for the formation of $H_2(v' = 1, j' = 1)$ and $H_2(v' = 1, j' = 3)$ at 11 collision energies between 0.88 and 1.01 eV, the region in which the two most pronounced resonances appear in the NV data (Fig. 2). We also measured the $H_2(v' = 1, j' = 3)/H_2(v' = 1, j' = 1)$ population ratio at two other values of E_{rel} outside this range. We found no sharp structure in the collision-energy dependence of the integral rate constants. There is excellent agreement between the results of the present experiment and the QM calculations of ZM for the dependence on E_{rel} of both the integral rate constants and the population ratio.[38]

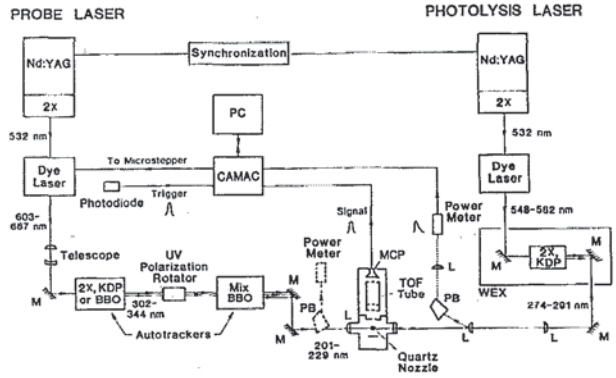

FIG. 3. Schematic diagram of the experimental configuration. M = dichroic mirror, L = lens, PB = Pellin–Broca prism, MCP = multichannel-plate detector, and PC = personal computer.

II. EXPERIMENT

The experimental apparatus and procedure were similar to those used in our studies of the $H + D_2$[39–41] and $D + H_2$[23,24] reactions. In this section we describe the experimental approach, with emphasis on the modifications relevant to the present study.

An overview of the experimental setup is shown in Fig. 3; the vacuum chamber is detailed in Fig. 4. HI and $p\text{-}H_2$ were premixed and effusively flowed into a high vacuum chamber via a capillary nozzle. The reaction was initiated ~2 mm below the nozzle by laser photolysis of $HI(\lambda_{ph} = 274\text{–}291\ \text{nm})$. After a delay of ~55 ns, the H_2 product was state-selectively ionized by a second laser ($\lambda_{probe} \approx 211$ nm) via $(2+1)$ REMPI.[42] The H_2^+ ions were mass-selectively detected in a shuttered time-of-flight mass spectrometer (TOF/MS).[41] The collision energy was varied by tuning the photolysis laser wavelength, and the $H_2(v', j')$ product states were detected by scanning the wavelength of the probe laser.

A. Reagents

HI (Matheson; 98.0% stated purity) was purified in a glass bulb by a freeze–pump–thaw cycle in order to remove the H_2 contaminant; most of the I_2 contaminant remained in the HI cylinder. The purified HI flowed into a 4 ℓ, Teflon-lined sample cylinder.

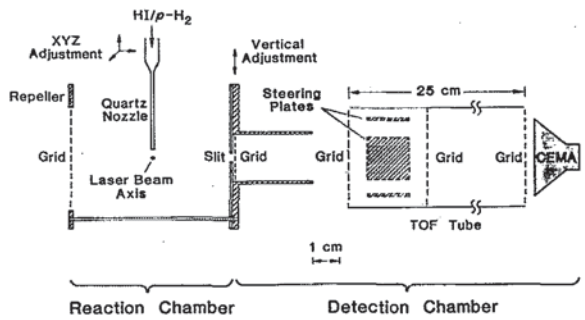

FIG. 4. Expanded view of the reaction and detection chambers.

Para-H_2 was generated by passing *normal*-H_2 (n-H_2) (Linde, 99.9995 +% stated purity) over an activated Ni salt-based catalyst (Houdricat 197-CP, Houdry Process and Chemical Co.) that had been cooled to liquid-H_2 temperature (~ 10 K) by being lowered into the neck of a liquid-He dewar. The p-H_2 generator, whose design was similar to that of Yu *et al.*,[43] consisted of two concentric stainless steel tubes (0.5 in. and 0.25 in. o.d.). The catalyst and a temperature-sensitive diode (Lake Shore Cryotronics) were at the bottom of the outer tube. The temperature was controlled by varying the depth of the generator in the dewar. The H_2 entered the generator through the 0.5 in. tube, was liquefied, passed over the catalyst, and flowed out through the 0.25 in. tube. A 2 μm stainless steel frit (Cajon) was press fit into the bottom of the inner tube to prevent the catalyst from being swept out of the p-H_2 generator. The p-H_2 warmed to room temperature (away from the catalyst) as it flowed from the generator into the sample cylinder that contained the purified HI. The total pressure (MKS Baratron) in the sample cylinder was ~ 1100 Torr, with a p-H_2/HI concentration ratio of $\sim 45/1$. The motivation for choosing this ratio is discussed in Sec. II. F.

The purity of the p-H_2, defined as $[p\text{-}H_2]/([p\text{-}H_2] + [o\text{-}H_2])$, was determined by flowing the reagent mix into the vacuum chamber via the nozzle (~ 200 mTorr backing pressure) and measuring the $H_2(v=0, j=5)$ and $H_2(v=0, j=6)$ populations with REMPI. The fractions of the total o-H_2 and p-H_2 populations occupying these levels are easily calculated from the room-temperature partition functions. Space-charge effects made it difficult to measure reliable populations of lower levels. Such measurements were occasionally made by lowering the nozzle backing pressure, and the same purity value was obtained. Another check on the method of determining the purity was provided by measuring the "p-H_2 purity" of n-H_2, which yielded a value of $\sim 25\%$,[44] thereby confirming that the above method provided an accurate determination of the p-H_2 purity.

It should be noted that the measured purity was slightly degraded by the presence of the small amount of HI. This degradation occurred via the reactions $H + HI \rightarrow H_2 + I$ and $H + p\text{-}H_2 \rightarrow o\text{-}H_2 + H$, which were initiated by probe-laser photolysis of HI (discussed in Sec. II D). This effect was expected to be minor because (a) the HI concentration was $\sim 2\%$ of the total and (b) the levels used in the purity measurement were dominated by the thermal reagent population rather than by the reactive contribution (as was confirmed by performing the purity measurement on other H_2 levels). Nonetheless, the measured p-H_2 purity constituted a lower limit.

For the present experiment, the measured p-H_2 purity was 97%–99% at the beginning of each experimental run and 95%–97% at the end. The purity was measured each time it was generated (before each experiment) and was checked at the end of every experimental run. From these measurements, the decay rate of p-H_2 in the gas handling and storage system was determined to be $\leqslant 0.5\%$/h. The decay rate in the absence of HI was found to be similar.

The p-H_2/HI mix was introduced into the reaction chamber (Fig. 4) via a vertical quartz capillary nozzle (~ 0.8 mm i.d. orifice), which was graphite coated and electrically grounded in order to minimize electrostatic charging. The pressure behind the nozzle was 6.0–10.0 Torr, regulated to $\pm 3\%$ by a bellows metering valve (Nupro). The corresponding pressure below the nozzle was $\leqslant 10$ mTorr. It has previously been verified that under these conditions the flow is effusive.[39] Hence, the rotational distribution of the 293 K p-$H_2(v=0)$ reagent was 0.525:0.460:0.015 for $j = 0$:2:4.

B. Lasers

The two laser systems are shown in Fig. 3. The photolysis laser consisted of a frequency-doubled Nd:YAG-pumped dye laser (Spectra-Physics, DCR-1A, PDL-1, WEX) operated with the dyes R575, R590, and R610 (Exciton), providing pulsed (10 Hz, ~ 5 ns pulse duration) tunable uv radiation from 274–291 nm. The uv light was separated from the dye fundamental and directed into the reaction chamber by a pair of dichroic mirrors (CVI Laser Corp.). The beam was telescoped to a diameter of ~ 3 mm before entering the chamber through a Suprasil window (Heraeus Amersil). The photolysis pulse passed ~ 2 mm below the tip of the nozzle (care was taken to ensure that the beam did not intersect the nozzle) and exited the chamber through a lens opposite the flat. The telescope was adjusted so that the beam was slightly divergent in order to minimize damage to the lens opposite the flat. The second lens of the telescope was mounted on an x–y–z translation stage to allow adjustment of the divergence and fine positioning of the photolysis beam.

The photolysis-laser power was measured after the beam exited the chamber by translating a Pellin–Broca (PB) prism into the beam path. The prism separated the residual visible light from the uv radiation, which was directed into a power meter (Scientech). The uv energy was measured to be 5–12 mJ per pulse. By removing the lens and flat that provided optical access to the reaction chamber, it was determined that the energy delivered to the photolysis region was 10%–25% higher than that measured after the chamber (depending on the age of the lens and flat).

The photolysis dye laser was scanned over the region 548–582 nm in steps of approximately 2 nm. The dye-laser readout was determined to be accurate to ± 4 Å by calibration against both red and green HeNe lasers. The corresponding uncertainty in E_{rel} was about ± 0.002 eV.

The probe laser system, used to detect the H_2 product of the $H + p$-H_2 reaction and to measure the p-H_2 purity via REMPI, was identical to that described in Ref. 40. It consisted of a pulsed (10 Hz, ~ 5 ns pulse duration) Nd:YAG-pumped dye laser (Spectra-Physics, DCR-3G, PDL-1; Exciton, R640/DCM dye mix) with frequency-doubling and mixing stages (INRAD Autotracker II). The dye laser light was frequency doubled and mixed in β-barium borate (BBO) crystals,[45] yielding ~ 1.5 mJ per pulse of tunable uv radiation (~ 211 nm for detecting the reaction product, ~ 203 nm for measuring the p-H_2 purity). Two dichroic mirrors (Virgo Optical) separated the

~200 nm radiation from the other wavelengths and steered the beam into the reaction chamber, collinear with and counterpropagating to the photolysis beam. The lens mounted on the chamber (Esco, Suprasil B, $f = 125$ mm) focused the probe beam to a small spot (100 μm estimated diameter) under the nozzle, after which the beam exited the chamber through the flat.

The probe-laser energy was measured (Molectron J3-09) using a back reflection of the probe beam from the second lens of the photolysis-laser telescope. The back reflection was passed through a PB prism to separate the probe light from other frequencies and was collimated.

The spatial overlap of the photolysis- and probe-laser beams was set coarsely using the dichroics in the photolysis-beam path. Fine adjustment was accomplished with the translatable lens of the photolysis-laser telescope. The latter optimization was performed on $H_2(v' = 1, j')$ signal from the H + HI reaction, which was more sensitive to small changes in signal intensity than H + p-H_2 signal because of the higher S/N ratio for the H + HI reaction.

It was important to use nondispersive optical elements to separate the dye-fundamental and doubled-dye wavelengths of the photolysis laser in order to avoid beam walk as λ_{ph} was tuned. As the wavelength was varied, it was confirmed that there was no measurable beam walk using (a) multiple irises placed in the photolysis beam path and (b) measurements of the $H_2(v' = 1, j')$ signal from the H + HI reaction. The experimental geometry was fairly tolerant of beam walk because the focused probe beam was overlapped with the relatively large, collimated photolysis laser beam. The overlap was checked on H + HI signal each day prior to collecting data, and it was found that the overlap often did not drift for several days.

The high-intensity uv laser pulses caused surface and bulk damage to the lens and flat mounted on the reaction chamber, diminishing the transmission of these optics. After typically ~100 hours of exposure to the lasers (~3.6 million shots from each laser), the lens and flat were removed to be cleaned and/or replaced, necessitating realignment of the laser beams and the nozzle.

C. Ion detection

The H_2^+ ions formed via REMPI were detected with a TOF/MS (Fig. 4), which was a modified version of that described in Refs. 40 and 41. The modifications were necessary in order to improve the S/N ratio to an acceptable level. In our previous studies of the H + D_2 and D + H_2 reactions, the $m/e = 3$ signal was uniquely that of the HD product. In the present experiment, the reagent and product masses were the same; the H_2^+ product ions had to be detected against an unresolved background of $m/e = 2$ "secondary" ions from other sources (primarily electron-impact ionization from electrons generated by scattered laser light). In our studies of the H + D_2 reaction, a similar problem was nearly eliminated by pulsing the voltage on one of the steering plates in the TOF/MS.[41] The pulsed plate acted as an ion "shutter," open to transmit only the mass of interest. For the present experiment, this shutter did not sufficiently reduce the noise caused by secondary ions. The following modifications (compare Fig. 4 with Fig. 2 of Ref. 41) significantly diminished the secondary-ion interference:

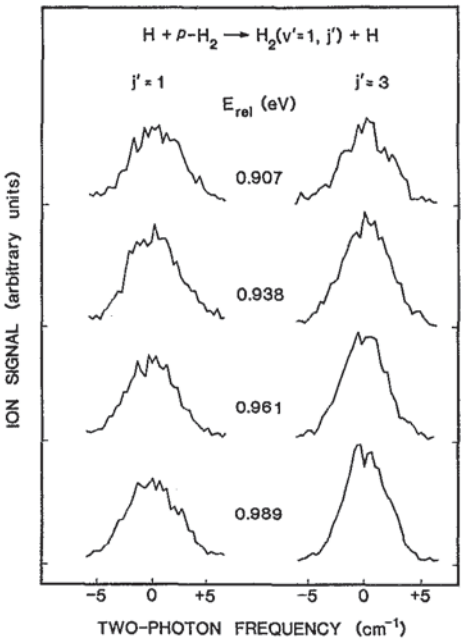

FIG. 5. Representative spectral peaks for the $H_2(v' = 1, j')$ product of the H + p-H_2 reaction. Each peak represents one scan, which took 220–330 s. See the text for additional experimental conditions. The spectra at $E_{rel} = 0.907$ and 0.938 eV were taken with R590 dye on one day and those at $E_{rel} = 0.961$ and 0.989 eV were taken with R575 dye on another day.

(1) The TOF tube was lengthened from 14 to 25 cm, improving the flight-time resolution.

(2) A grid at the same voltage as the TOF tube was installed before the steering plates. This grid diminished the time during which the pulsed plate interacted with the ions prior to their arrival at the plate, allowing the pulse length to be shortened and thereby diminishing the number of secondary ions passing through the shutter.

(3) The voltage on the repeller plate was pulsed from ground to about 400 V several ns prior to the firing of the probe laser, but after the firing of the photolysis laser. This modification improved the definition of the time of formation of the ions to be detected by TOF. It was particularly effective in reducing interference from secondary ions created in conjunction with the photolysis laser.

The ion signal from the CEMA detector (Galileo) was measured by a computer-interfaced CAMAC system[46] that gated (35 ns width) and integrated the H_2^+ ion current. The spectra were recorded with a 4–6 s time constant. Typical spectra are shown in Fig. 5.

The REMPI-TOF/MS detection scheme was calibrated against a high-temperature, effusive nozzle source of H_2. The calibration is described in separate publications.[42] No correction factors were required for the levels detected in the present study, i.e., the integrated ion signals (corrected for probe-laser power) were directly proportional to quantum-state populations.

TABLE I. HI photolysis parameters.

λ_{ph}(nm)[a]	σ (arb. units)[b]	I*/I[b]	E_{rel} (eV) H + p-H_2[c]	H + HI[d]
291.00	2079	0.0159	0.828	1.213/0.285
285.00	3115	0.0560	0.887	1.302/0.373
283.95	3324	0.0678	0.898	1.318/0.389
283.00	3523	0.0802	0.907	1.332/0.404
281.90	3763	0.0968	0.919	1.349/0.420
281.00	3969	0.1122	0.928	1.363/0.434
280.00	4208	0.1315	0.938	1.378/0.450
279.00	4459	0.1533	0.949	1.394/0.465
277.87	4758	0.1812	0.961	1.412/0.483
276.60	5119	0.2174	0.974	1.432/0.503
275.27	5524	0.2605	0.989	1.453/0.525
274.00	5944	0.3075	1.003	1.474/0.545
~211[e]	27000	0.36	1.90/1.28	2.80/1.88

[a]Uncertainty is about ±0.2 nm.
[b]From Ref. 48.
[c]Uncertainty is about ±0.002 eV; spread is about 0.3 eV FWHM. See the text.
[d]The two collision energies at each λ_{ph} correspond to the production of the two I-atom spin–orbit states. Uncertainty is about ±0.003 eV; spread is about 0.08 eV (0.04 eV) FWHM for the fast (slow) channel.
[e]Prompt reaction; see the text.

D. Probe-laser-induced reaction

As in our studies of the H + D_2 system, we observed a probe-laser-induced ("prompt") reaction in which the probe laser both photodissociated HI and detected the H_2 product formed during a single laser pulse.[39] The contribution of the prompt reaction to the total ion signal was subtracted on a shot-by-shot basis, as detailed in Ref. 40 (method 2). Briefly, the delay between the photolysis and probe laser pulses was switched between ~15 and ~55 ns on alternate shots. The signal had the same prompt-reaction contribution at both delays, but had a larger contribution from the photolysis-laser-induced reaction at the longer delay because of product buildup. Thus, subtraction of the ion signal at ~15 ns delay from that at ~55 ns delay contained signal exclusively from the photolysis-laser-induced reaction (see Ref. 40). The spectra shown in Fig. 5 and the subsequent tables and graphs of the data have been corrected for the prompt-reaction background using this procedure. A spectral peak recorded with a 5 s time constant corresponded to 25 shots each taken at the short and long delays for each point in the spectrum.

E. HI photolysis

The photodissociation of HI[47,48] (Table I) produces both ground state $I(^2P_{3/2}) \equiv I$ and spin–orbit excited $I(^2P_{1/2}) \equiv I^*$, with the corresponding production of two groups of H atoms with different speeds. For all of the photolysis wavelengths employed in the present study (except that of the prompt reaction), the slow H atoms produced in coincidence with I* had insufficient energy to populate $H_2(v'=1)$ product levels. Thus, the measured rate constants were derived from a unimodal collision-energy distribution. For the prompt reaction ($\lambda_{ph} \approx 211$ nm), the two collision energies were 1.90 and 1.28 eV and the I*/I branching ratio has been calculated to be 0.26/0.74.[48] The prompt rate constants therefore consisted of 74% of the 1.90 eV rate constant plus 26% of the 1.28 eV rate constant (78% of the 1.90 eV cross section plus 22% of the 1.28 eV cross section).

Although the collision-energy distribution was unimodal for the present experiment, the width of this distribution was large, as has been shown by van der Zande *et al.*[37] (see Sec. I). The H + H_2 E_{rel} distribution was nearly Gaussian with a FWHM of 0.3 eV under our experimental conditions. Note that for most of the range of E_{rel} covered in the present study, the spacing between adjacent E_{rel} values was small relative to this width. Such a fine energy grid was required for comparison with the experiment of NV.

F. Experimental checks and data analysis

In the course of our previous measurements on the H + D_2 reaction, studies were performed to ensure that the observed signal was from the nascent HD reaction product.[40] For the present experiment, which was performed under conditions similar to those of the H + D_2 experiment, several additional checks were required in order to characterize the system. Measurements pertaining to p-H_2 purity and photolysis-laser beam walk have already been discussed in Secs. II A and II B, respectively.

The rate of product buildup for the reaction H + p-$H_2 \rightarrow o$-$H_2(v', j')$ + H is given by

$$\frac{d[o\text{-}H_2(v',j')]}{dt} = k_{v'j'}[H][p\text{-}H_2], \tag{1}$$

where $[i]$ denotes the number density of species i and $k_{v'j'}$ is the integral, specific rate constant (the quantity to be determined in the present experiment). For short times Δt integration of Eq. (1) gives

$$k_{v'j'} = [o\text{-}H_2(v',j')]/[H][p\text{-}H_2]\Delta t. \tag{2}$$

Under our experimental conditions, $[p\text{-}H_2]$ and Δt (the delay between the photolysis and probe lasers) were constants. The measured REMPI ion signal, $S_{v'j'}$ (integrated and corrected for probe-laser power), was proportional to $[o\text{-}H_2(v',j')]$. Therefore,

$$k_{v'j'} = CS_{v'j'}/[H], \tag{3}$$

where C is a constant.

The rate constant $k_{v'j'}$ as a function of E_{rel} was obtained by correcting $S_{v'j'}$ for variations in [H] with λ_{ph}, as described below. Because the value of the constant C in Eq. (3) was unknown, this procedure yielded relative, not absolute, rate constants.

1. Variation of H-atom density with λ_{ph}

Both the HI absorption cross section σ and the I*/I branching ratio varied significantly over the present range of λ_{ph} (Table I). Between λ_{ph} = 285 and 274 nm, σ increased by nearly a factor of 2 and the contribution of the I* channel increased from 5% to 24%.[48] In addition, the photolysis-laser power varied by almost a factor of 2 as λ_{ph}

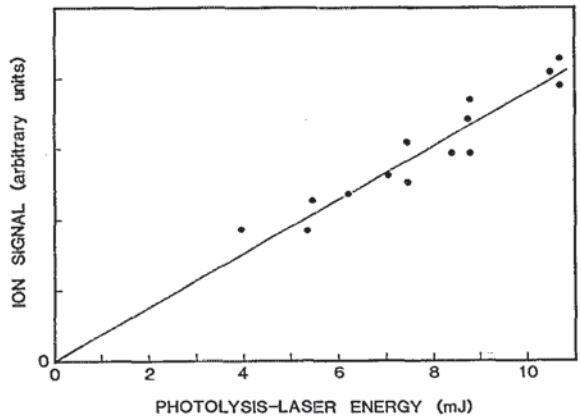

FIG. 6. Integrated REMPI signal as a function of photolysis-laser energy at $\lambda_{ph} = 276.60$ nm for the reaction $H + p\text{-}H_2 \rightarrow H_2(v' = 1, j' = 3) + H$. Points are experimental (two scans over the spectral peak at each energy); line is a linear-least-squares fit constrained to go through the origin.

was tuned over the dye gain curves. These variations affected the density of the H-atom reagent produced by the photolysis laser and therefore had to be included in the data analysis [see Eq. (3)].

The H-atom number density [H] produced by the photolysis laser for a particular photolysis channel is given by

$$[H] = [HI]_0(1 - e^{-I\sigma f\delta}), \tag{4}$$

where $[HI]_0$ is the initial HI number density, I is the photon flux, σ is the HI absorption cross section, f is the branching ratio into the channel of interest, and δ is the duration of the laser pulse. We calculate that $\sim 5\%$ of the HI was photolyzed under our experimental conditions, in which case [H] was expected to be linear with photolysis energy. Performing a Taylor series expansion of the exponential in Eq. (4), inserting the result into Eq. (3), and absorbing the constants $[HI]_0$ and δ into C yields

$$k_{v'j'} = C' S_{v'j'}/If\sigma. \tag{5}$$

Equation (5) shows that $S_{v'j'}$ should depend linearly on photolysis energy (proportional to I). This conjecture was verified by measuring the photolysis-laser power dependence of the $H_2(v' = 1, j' = 3)$ signal from the $H + p\text{-}H_2$ reaction. The energy of the photolysis laser was varied over a range in excess of that encountered in the $H + p\text{-}H_2$ reactive measurements by inserting both neutral density filters into the photolysis beam and thin, glass, microscope slide covers into the amplifier pump beam of the dye laser. Such power-dependence determinations were performed at two different photolysis wavelengths because σ and f varied significantly over the present range of λ_{ph}. A representative measurement is shown in Fig. 6, in which it is seen that the ion signal was linearly proportional to the photolysis-laser energy. These measurements, which were carried out several times over the course of the experiment, verified that Eq. (5) provided the correct prescription for analyzing the data.

Thus, the rate constants $k_{v'j'}$ were obtained by dividing the measured ion signals by the photolysis-laser power and by $f\sigma$ [Eq. (5)]. The fraction, f, of the total absorption cross section that accessed the relevant I-atom channel was obtained simply from the I*/I branching ratio according to

$$f = (1 + I^*/I)^{-1}. \tag{6}$$

Values of σ and I*/I from the theoretical calculation of Levy and Shapiro[48] were used; an insufficient number of experimental values have been determined to provide a more reliable interpolation than that provided by the computation.

2. Interference from the H+HI reaction

A major complication in the current experiment, which is not present in studies of isotopic analogs of the $H + H_2$ reaction, was contamination by the H + HI reaction, i.e., $o\text{-}H_2$ could originate from two reactions: $H + p\text{-}H_2 \rightarrow o\text{-}H_2 + H$ and $H + HI \rightarrow o\text{-}H_2 + I$. The H + HI contribution to the total signal had to be quantified, suppressed, and eventually subtracted. It was deemed impractical experimentally to eliminate completely the H + HI reaction. $H_2(v' = 1, j')$ spectra were recorded as a function of the $p\text{-}H_2/HI$ concentration ratio, from $p\text{-}H_2/HI = 0/1$ (pure HI) to 65/1. The ion signal diminished monotonically with decreasing HI concentration. Similar measurements were performed with He substituted for the $p\text{-}H_2$ in order to isolate the H + HI contribution to the total signal. In the latter measurements, the H_2 signal from the H + HI reaction was quadratic with HI partial pressure, as expected. Maximum suppression of the H + HI reaction required operating at the largest $p\text{-}H_2/HI$ ratio possible, while still maintaining adequate S/N. The $p\text{-}H_2/HI$ ratio chosen for the reactive measurements was 45/1; the H + HI contribution was determined to be $\sim 5\%$ of the total signal under this condition (see Sec. III).

The contamination of the $H + p\text{-}H_2$ measurements by the H + HI reaction, while small, was systematic. Experiments were performed to allow the subtraction of the H + HI contribution. The $H + HI \rightarrow H_2(v' = 1, j' = 1$ and $3) + I$ integral rate constants were measured as a function of E_{rel} at the same photolysis wavelengths as were employed in the $H + p\text{-}H_2$ measurements, i.e., the $H + p\text{-}H_2$ experiment was repeated for the H + HI reaction (see Sec. II E). By again substituting He for $p\text{-}H_2$ in the 45/1 ratio used in the $H + p\text{-}H_2$ measurements, the H + HI contribution to the $H_2(v' = 1, j' = 3)$ signal at $\lambda_{ph} = 280.0$ nm was determined to be $8.0 \pm 1.0\%$. Knowing the $H_2(v', j')$ relative rate constants from both the $H + p\text{-}H_2$ and H + HI reactions, and having absolutely related them at a single value of λ_{ph}, we were then able to subtract the H + HI contribution at all photolysis wavelengths.

3. I-atom MPI

Many I-atom MPI resonances exist in the present range of λ_{ph}. I^+ production was greatly enhanced when λ_{ph} was tuned to one of these wavelengths, causing substantial space-charge effects. These effects, such as shifting and broadening of the arrival time of the H_2^+ signal in the

TOF/MS, made it impossible to obtain reliable measurements at these photolysis wavelengths. Hence, all measurements were performed at wavelengths that did not coincide with I-atom MPI resonances. Although it was important that this limitation be recognized, it was not a severe constraint because these resonances are very sharp (in wavelength).

G. Experimental protocol

The E_{rel} region of interest (0.887–1.003 eV, 11 E_{rel} values) was divided into two ranges: (A) E_{rel} = 0.887–0.961 eV (eight values) and (B) E_{rel} = 0.949–1.003 eV (five values), corresponding to the dye gain curves of R590 and R575, respectively (Table I). The ranges were overlapped at two values of E_{rel} (0.949 and 0.961 eV). For each range, the following experimental protocol was repeated 15 times:

(1) HI was purified.
(2) The overlap of the laser beams was checked using H_2 signal from the H + HI reaction.
(3) Sufficient p-H_2 was generated for a p-H_2/HI ratio of 45/1.
(4) The p-H_2 purity was measured.
(5) The photolysis laser was scanned over the appropriate range. At each λ_{ph}, $H_2(v'=1, j'=1)$ and $H_2(v'=1, j'=3)$ spectra were recorded twice each, and the photolysis laser power was measured.
(6) $H_2(v'=1, j'=1)$ and $H_2(v'=1, j'=3)$ spectra were recorded at the first value of λ_{ph} to ensure that there had not been any drift.
(7) The p-H_2 purity was remeasured.

In step (5), the collision energy was not scanned monotonically in order of increasing or decreasing energy. For range *A*, e.g., the eight E_{rel} values (numbered by increasing energy) were scanned in the order 2, 4, 6, 8, 1, 3, 5, 7. This provided a particularly sensitive check for long-term drift, which would be visible as an intensity alternation between adjacent populations when plotted as a function of E_{rel}.

For range *A*, one run through the above protocol took 8–10 h and used the entire reservoir ($\sim$5 *l* atm) of reagents. For range *B*, 2–3 runs over the five E_{rel} values could be accomplished with each reagent fill; for this range step (6) was omitted, being redundant.

Step (5) of the protocol was followed for the H + HI reactive measurements, with seven runs being performed over each range of E_{rel}. Of course, for a given λ_{ph}, E_{rel} was different for H + HI than for H + H_2 because of the different reduced masses of the H_2I and H_3 systems (Table I).

The $H_2(v'=1, j'=3)/H_2(v'=1, j'=1)$ population ratio from the H + p-H_2 reaction was also measured at two values of E_{rel} outside of the above region, at λ_{ph} = 291.0 nm (E_{rel} = 0.828 eV) and at $\lambda_{ph} \approx$ 211 nm (prompt reaction, E_{rel} = 1.90/1.28 eV). For these measurements, experimental conditions were chosen such that no correction for the H + HI contribution was required. At λ_{ph} = 291.0 nm a p-H_2/HI ratio of 150/1 was used, at which dilution the H + HI contribution was immeasurably small. In the case of the prompt reaction, most of the HI was photolyzed and the reaction time was shorter than for the photolysis-laser-induced reaction, giving less time for product buildup; the H + HI contribution to the prompt signal was also immeasurably small. Because these two population-ratio measurements were not to be related to measurements at other photolysis wavelengths, no corrections for photolysis-laser energy, HI absorption cross section, or I*/I branching ratio were required.

TABLE II. Rate constants and population ratios.

	H + p-H_2 → $H_2(v'=1, j')$ + H		
	Relative rate constants[b]		$H_2(v'=1, j'=3)$/ $H_2(v'=1, j'=1)$
E_{rel}(eV)[a]	$j'=1$	$j'=3$	Population ratio[b]
0.828	...	...	0.65(14)
0.887	146(20)	116(20)	0.80(17)
0.898	141(08)	120(16)	0.85(12)
0.907	145(12)	129(13)	0.89(12)
0.919	141(11)	129(11)	0.91(10)
0.928	145(11)	135(14)	0.93(12)
0.938	146(13)	140(10)	0.96(11)
0.949	152(15)	161(18)	1.06(16)
0.961	158(12)	175(11)	1.11(11)
0.974	149(09)	176(09)	1.18(10)
0.989	153(09)	189(11)	1.24(11)
1.003	167(12)	220(11)	1.32(11)
1.90/1.28[c]	...	...	1.87(06)

[a]Uncertainty is about ±0.002 eV; spread is about 0.3 eV FWHM. See the text.
[b]Numbers in parentheses denote 1 standard deviation.
[c]Prompt reaction; see the text.

III. RESULTS

The H + p-H_2 → $H_2(v'=1, j')$ + H integral rate constants, derived from spectra such as those shown in Fig. 5, are tabulated in Table II and graphed as a function of E_{rel} in Fig. 7(a). The reported error bars represent one standard deviation of 15 scans over the region of interest, along with errors propagated in the subtraction of the H + HI contribution (uncertainties both from the H + HI measurements themselves and from the absolute locking of the H + HI and H + p-H_2 rate constants). They do not include any errors in the calculated HI absorption cross sections or I*/I branching ratios,[48] which were used in correcting the ion signal for changes in H-atom density with λ_{ph} (Sec. II F 1). If the calculated I*/I branching ratio were in error by 20%, which seems unlikely,[48] the corresponding error in the experimentally determined rate constant would be 1% at E_{rel} = 0.887 eV and 5% at E_{rel} = 1.003 eV [calculated via Eqs. (5) and (6)].

The dependence on E_{rel} of the H + p-H_2 integral rate constants is very flat and structureless between 0.88 and 1.01 eV, as shown in Fig. 7(a). The $H_2(v'=1, j'=1)$ rate constant is nearly independent of collision energy over this range, while the $H_2(v'=1, j'=3)$ rate constant increases slowly with increasing energy.

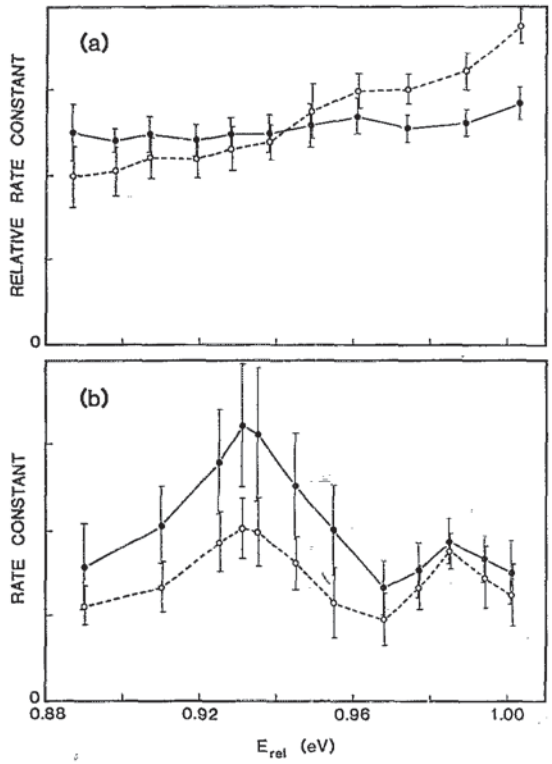

FIG. 7. Integral rate constants for the reaction $H + p\text{-}H_2 \rightarrow H_2(v' = 1, j') + H$ as a function of collision energy for $j' = 1$ (solid circles) and $j' = 3$ (open circles). (a) The results of the present study and (b) the absolute rate constants of NV. Error bars represent 1 standard deviation.

The $H_2(v' = 1, j' = 3)/H_2(v' = 1, j' = 1)$ population ratio as a function of E_{rel} is given in Table II and plotted in Fig. 8. Again, the error bars represent 1 standard deviation. The population ratio increases monotonically with increasing E_{rel} between 0.82 and 1.01 eV, crossing unity at $E_{rel} = 0.93 \pm 0.03$ eV.

The correction for the H + HI reaction had a more pronounced effect on the $H_2(v' = 1, j' = 3)/H_2(v' = 1, j' = 1)$ population ratios than on the rate constants. Since the E_{rel} dependence of the $H + HI \rightarrow H_2 + I$ integral rate constants is flat over the present range of interest (Table III), the correction had a negligible effect on the E_{rel} dependence of the $H + p\text{-}H_2$ rate constants [Fig. 7(a)]. However, the $H_2(v' = 1, j' = 3)/H_2(v' = 1, j' = 1)$ population ratio is ~ 2 for the H + HI reaction (Table III), but is approximately unity for the $H + p\text{-}H_2$ reaction. Therefore, the correction noticeably shifted the measured population ratio (Fig. 8). Although this shift (of a few percent) was within error bars, it was systematic and thus important to take into consideration. The H + HI contribution to the measured $H_2(v' = 1, j')$ populations was 5.6% on average; the average contribution to $j' = 1(j' = 3)$ levels was 3.7%(7.5%).

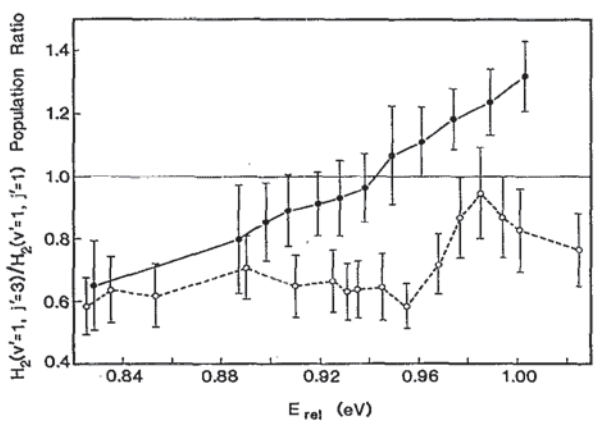

FIG. 8. The $H_2(v' = 1, j' = 3)/H_2(v' = 1, j' = 1)$ population ratio as a function of collision energy for the reaction $H + p\text{-}H_2 \rightarrow H_2(v' = 1, j') + H$. Solid circles are the results of the present study; open circles are the experimental results of NV. Error bars represent 1 standard deviation.

TABLE III. Rate constants and population ratios.

$H + HI \rightarrow H_2(v' = 1, j') + I$				
E_{rel}(eV)		Relative rate constants[a]		$H_2(v' = 1, j' = 3)/H_2(v' = 1, j' = 1)$
H + HI	$H + p\text{-}H_2$	$j' = 1$	$j' = 3$	Population ratio[a]
1.302/0.373	0.887	133(07)	293(19)	2.20(18)
1.318/0.389	0.898	136(11)	290(10)	2.14(18)
1.332/0.404	0.907	135(11)	281(15)	2.09(21)
1.349/0.420	0.919	139(13)	290(13)	2.09(22)
1.363/0.434	0.928	140(09)	311(13)	2.22(16)
1.378/0.450	0.938	146(06)	314(10)	2.15(11)
1.394/0.465	0.949	144(06)	312(23)	2.17(18)
1.412/0.483	0.961	150(12)	320(15)	2.13(19)
1.432/0.503	0.974	149(05)	323(14)	2.18(12)
1.453/0.525	0.989	152(08)	340(19)	2.23(17)
1.474/0.545	1.003	157(08)	345(17)	2.19(16)

[a]Numbers in parentheses denote 1 standard deviation.

As part of our preliminary measurements and because of the substantial disagreement between the present results and those of NV (see Sec. IV), several experiments were performed in order to check for systematic errors and to verify that the measured H_2^+ signals arose from the *o*-H_2 product of the $H + p\text{-}H_2$ reaction. These checks, which were discussed in Sec. II, included measurements related to the *p*-H_2 purity and decay rate in the gas handling and storage system, beam walk as λ_{ph} was tuned, the photolysis-power dependence of the ion signal, long-term stability of the signal, the H + HI contribution to the total signal, and interference from I-atom MPI resonances. In addition, the $H + p\text{-}H_2$ reactive measurements were repeated many times (15 repetitions for each range of E_{rel}) on different days; after several reactive runs, the system was completely realigned after replacing the optics that provided access to the vacuum chamber. From the results of these experimental checks and from the reproducibility of the measurements (reflected in the error bars), we conclude that the rate constants listed in Table II and plotted in Fig. 7(a) accurately represent the integral rate constants for the formation of *o*-H_2 from the $H + p\text{-}H_2$ reaction.

IV. DISCUSSION

A. Comparison with previous experiment

The present results are directly comparable to those of NV (see Sec. I). The $H_2(v' = 1, j' = 1)$ and $H_2(v' = 1,$

$j' = 3$) integral rate constants as a function of E_{rel} obtained from the present experiment are shown in Fig. 7(a) and those reported by NV are shown in Fig. 7(b). To obtain the rate constants in Fig. 7(b), NVs reported cross sections, which had been derived from measured rate constants,[29] were multiplied by $(E_{rel})^{1/2}$. None of the sharp structure observed by NV is found in the present experiment. Figure 8 displays a comparison of the $H_2(v' = 1, j' = 3)/H_2(v' = 1, j' = 1)$ population ratios. The results of the two experiments are discordant. We have been informed that a reinterpretation of the NV experiment is in progress.[36,49]

B. Implications for the experimental observation of dynamical resonances

The present results have implications for the observation of dynamical resonances in $H + p\text{-}H_2$ reactive scattering experiments. It is evident from the QM calculations that resonances exist in the $H + p\text{-}H_2$ reaction.[12–14] However, the averaging over partial scattering waves inherent in an integral cross section measurement, even one that has full reactant and product quantum-state resolution, is sufficient to eliminate the sharp resonance structure (see Fig. 1). The remaining weak undulations in the E_{rel} dependence of the integral cross sections (see Fig. 2) would be difficult to quantify experimentally and, if observed, to ascribe to dynamical resonances. The substantial, superthermal energy spread of bulb experiments[37] further diminishes any energy dependence of the integral cross sections. Moreover, the QM calculations indicate that, even for an experiment with perfect energy resolution, resonances in the $H + p\text{-}H_2$ reaction would be difficult to detect in an integral-cross-section measurement.[50] The extent to which QM effects influence the shapes of the integral cross sections as a function of E_{rel} can only be determined by comparison with corresponding classical calculations; such calculations are not currently available.

Continetti, Zhang, and Miller[51] recently reanalyzed the QM calculations of Zhang and Miller[15] for the $D + H_2$ reaction. This analysis indicated that dynamical scattering resonances should be observable in a measurement of doubly differential cross sections for this system, i.e., in an experiment that resolves both the internal state and the scattering angle of the HD product.[52] To date, no such measurements have been reported for any isotopic variant of the $H + H_2$ reaction. Current experiments have either full internal state and no angular resolution[21–24,39,40] or angular and only partial internal state resolution.[25,26,53,54]

C. Comparison with quantum-mechanical calculations

The present results can also be compared with the fully converged, three-dimensional QM calculations of ZM. In order to make the comparison as quantitative as possible, the QM cross sections were averaged over the experimental collision-energy spread (see Secs. I and II E). First, a cubic spline fit to the QM cross sections as a function of E_{rel} was performed, a procedure that seems valid in light of the smooth dependence on collision energy of the converged QM cross sections. These cross sections were then converted to rate constants (the experimentally measured quantity), and the rate constants were convolved with a 0.3 eV FWHM Gaussian. We compare with these convolved, integral rate constants in Fig. 9. Since we measured relative rate constants, the following normalization has been employed: the weighted sum of the 22 experimental rate constants was set equal to the corresponding sum of the theoretical rate constants (i.e., the normalization has not been biased to any particular final state or collision energy). The agreement between experiment and QM theory is excellent, with the QM predictions agreeing with 19 of the 22 experimental points within the 1-standard-deviation experimental error bars.

The dependence on E_{rel} of the $H_2(v' = 1, j' = 3)/H_2(v' = 1, j' = 1)$ population ratio is shown in Fig. 10.

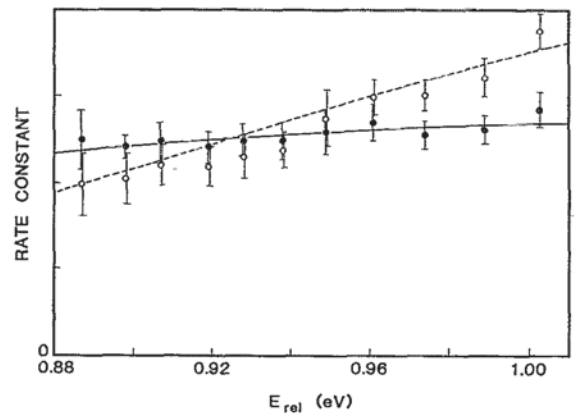

FIG. 9. Integral rate constants for the reaction $H + p\text{-}H_2 \rightarrow H_2(v' = 1, j') + H$ as a function of collision energy for $j' = 1$ (solid circles and solid curve) and $j' = 3$ (open circles and dashed curve). Points are the results of the present experiment; curves are the QM results of ZM. The experimental data have been normalized such that the sum of the 22 measured rate constants equals the corresponding theoretical sum. Error bars represent 1 standard deviation.

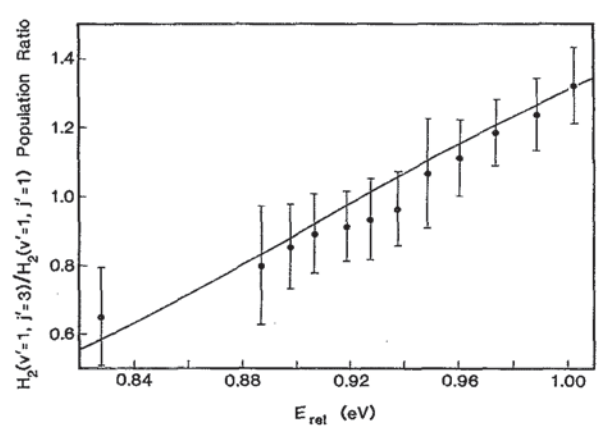

FIG. 10. The $H_2(v' = 1, j' = 3)/H_2(v' = 1, j' = 1)$ population ratio as a function of collision energy for the reaction $H + p\text{-}H_2 \rightarrow H_2(v' = 1, j') + H$. Points are the results of the present study; curve is the QM result of ZM. Error bars represent 1 standard deviation.

There is outstanding agreement between experiment and QM theory for all 12 values of E_{rel}. The calculated population ratio crosses unity at $E_{rel} = 0.925$ eV, in excellent accord with the experimental value of 0.93 ± 0.03 eV. It should be noted that no normalization has been employed in this comparison. Hence, such a quantity has the advantage of an absolute measurement (in that no normalization is required to compare different experiments or theory with experiment) while retaining the smaller error bars characteristic of a relative measurement. There are presently no calculations available to extend the comparison of Fig. 10 to the E_{rel} values accessed by the prompt reaction (Table II, last entry).

In making the comparisons shown in Figs. 9 and 10, it must be noted that even after the convolution over the experimental energy spread, the calculations and measurements refer to slightly different initial conditions. In the experiment, the p-H_2 reagent was thermal ($v = 0$; 52.5% $j = 0$, 46.0% $j = 2$, 1.5% $j = 4$), while in the computation the initial state was exclusively ($v = 0$, $j = 0$). However, recent QM calculations indicate that the effect of j on the integral cross sections is minor for the energies and initial rotational states accessed in the present experiment.[18,55] In addition, the p-H_2 reagent contained a few percent o-H_2 contamination, which could populate the measured product levels by both inelastic and reactive scattering. Nonetheless, the experimental and theoretical initial conditions were sufficiently similar that a comparison was appropriate.

The agreement shown in Figs. 9 and 10 is reminiscent of that observed in the comparison of our previous results with those of QM theory for the reaction $D + H_2(v = 0, j$ thermal$) \rightarrow HD(v' = 1, j') + H$,[24] in which two QM calculations reproduced the measured rotational distribution nearly perfectly. That study indicated that the current level of QM reactive scattering theory is adequate to describe quantitatively some aspects of the $H + H_2$ reaction dynamics, although the generality of that conclusion could not be assessed from the results of a single experiment. The results of the present experiment further support that conclusion. Similarly, the QM value[15] of the total cross section for the reaction $D + H_2(v = 1, j = 0) \rightarrow HD + H$ at $E_{rel} = 0.33$ eV agrees with that determined experimentally by Götting *et al.*[20] within experimental uncertainty.

Not all comparisons between experiment and QM theory have produced quantitative agreement such as that shown in Figs. 9 and 10 and Refs. 15 and 24. Kliner and Zare[23] recently reported experimental results for the reaction $D + H_2(v = 1, j = 1) \rightarrow HD(v' = 1, j') + H$ at $E_{rel} = 1.0$ eV, in which the H_2 reagent was rovibronically state selected. Vibrational excitation of the H_2 reagent resulted in substantial internal excitation of HD product. This trend was reproduced in the QM calculations of Blais *et al.*,[17] and the first moments derived from experiment and theory agreed very well ($\langle j' \rangle_{v'=1} \approx 8$). However, the shapes of the measured and calculated rotational distributions were not in quantitative agreement. Further experiments are required to determine if this discrepancy will persist after removal of the approximations used in the analysis of the experimental data.

All of the above measurements refer to integral cross sections. In contrast, two groups have reported crossed-beam studies of the $D + H_2$ reaction, in which vibrational-state-resolved differential cross sections of the HD product were obtained. Buntin, Giese, and Gentry[25,53] measured HD TOF distributions at a fixed laboratory scattering angle for six values of E_{rel} between 0.85 and 1.20 eV. Continetti, Balko, and Lee[26] performed similar measurements at many scattering angles for $E_{rel} = 0.53$ and 1.01 eV. After averaging the QM results of Zhang and Miller[15] (performed on the LSTH[30] PES) and of Zhao *et al.*[18] (DMBE[31] PES) over their respective experimental resolution functions, both groups found good overall agreement between QM theory and experiment. However, they noted differences between the calculated and measured TOF distributions that were outside of experimental uncertainty. These workers[25,26] suggested that the discrepancies were caused by inaccuracies in the H_3 PESs used in the QM computations, with emphasis on possible errors in the calculated bend potentials.

Because of the recent advances in experimental and theoretical methodologies for treating the $H + H_2$ reaction family, detailed comparisons between QM calculations and experimental measurements are now possible. In particular, several experimental techniques[27] have opened the possibility of probing the H_3 PES in a more global fashion and with increasing detail. Corresponding theoretical results[19] at the (relatively high) energies accessed in the experiments and over a broad range of initial conditions allow detailed simulations of the experiments to be performed. Further comparisons between QM theory and experiment, which are required for a more complete understanding of this benchmark reaction, should be forthcoming.

ACKNOWLEDGMENTS

We thank J. Z. H. Zhang and W. H. Miller for providing us with a tabulation of their calculated $H + p$-H_2 reactive cross sections, and I. Levy and M. Shapiro for providing us with a tabulation of their calculated HI absorption cross sections and I*/I branching ratios. We are grateful to C. Chiladakis (Low Temperature Laboratory, Chemistry Department, UC Berkeley) and L. E. Dillard (Physics Department, Stanford University) for assistance in the design of the p-H_2 generator, and to R. P. Dorricott (Sunnyvale Valve and Fitting) for supplying the frit for the p-H_2 generator. This work was supported by the National Science Foundation under NSF CHE 90-07939.

[1] A. Kuppermann, in *Potential Energy Surfaces and Dynamics Calculations*, edited by D. G. Truhlar (Plenum, New York, 1981).
[2] B. C. Garrett, D. W. Schwenke, R. T. Skodje, D. Thirumalai, T. C. Thompson, and D. G. Truhlar, in *Resonances in Electron–Molecular Scattering, van der Waals Complexes, and Reactive Chemical Dynamics*, edited by D. G. Truhlar, ACS Symposium Series 263 (American Chemical Society, Washington DC, 1984).
[3] G. C. Schatz, Ann. Rev. Phys. Chem. **39**, 317 (1988).
[4] D. M. Neumark, A. M. Wodtke, G. N. Robinson, C. C. Hayden, and Y. T. Lee, J. Chem. Phys. **82**, 3045 (1985); D. M. Neumark, A. M.

Wodtke, G. N. Robinson, C. C. Hayden, K. Shobatake, R. K. Sparks, T. P. Schafer, and Y. T. Lee, *ibid.* **82**, 3067 (1985).
[5] D. G. Truhlar and A. Kuppermann, J. Chem. Phys. **52**, 3841 (1970); **56**, 2232 (1972); G. C. Schatz and A. Kuppermann, *ibid.* **59**, 964 (1973).
[6] S.-F. Wu and R. D. Levine, Chem. Phys. Lett. **11**, 557 (1971); Mol. Phys. **22**, 881 (1971).
[7] G. C. Schatz and A. Kuppermann, Phys. Rev. Lett. **35**, 1266 (1975).
[8] G. C. Schatz, Chem. Phys. Lett. **94**, 183 (1983).
[9] D. Neuhauser, R. S. Judson, R. L. Jaffe, M. Baer, and D. J. Kouri, Chem. Phys. Lett. (in press).
[10] I. M. Waller, T. N. Kitsopoulos, and D. M. Neumark, J. Phys. Chem. **94**, 2240 (1990), and references therein.
[11] M. Mladenovic, M. Zhao, D. G. Truhlar, D. W. Schwenke, Y. Sun, and D. J. Kouri, J. Phys. Chem. **92**, 7035 (1988).
[12] J. Z. H. Zhang and W. H. Miller, Chem. Phys. Lett. **153**, 465 (1988).
[13] D. E. Manolopoulos and R. E. Wyatt, Chem. Phys. Lett. **159**, 123 (1989).
[14] J. M. Launay and M. Le Dourneuf, Chem. Phys. Lett. **163**, 178 (1989).
[15] J. Z. H. Zhang and W. H. Miller, J. Chem. Phys. **91**, 1528 (1989).
[16] D. E. Manolopoulos and R. E. Wyatt, J. Chem. Phys. **92**, 810 (1990).
[17] N. C. Blais, M. Zhao, D. G. Truhlar, D. W. Schwenke, and D. J. Kouri, Chem. Phys. Lett. **166**, 11 (1990).
[18] M. Zhao, D. G. Truhlar, D. W. Schwenke, and D. J. Kouri, J. Phys. Chem. **94**, 7074 (1990); see also, M. Zhao, D. G. Truhlar, D. J. Kouri, Y. Sun, and D. W. Schwenke, Chem. Phys. Lett. **156**, 281 (1989).
[19] W. H. Miller, Ann. Rev. Phys. Chem. **41**, 245 (1990), and references therein.
[20] R. Götting, V. Herrero, J. P. Toennies, and M. Vodegel, Chem. Phys. Lett. **137**, 524 (1987).
[21] J.-C. Nieh and J. J. Valentini, Phys. Rev. Lett. **60**, 519 (1988); J. Chem. Phys. **92**, 1083 (1990).
[22] D. L. Phillips, H. B. Levene, and J. J. Valentini, J. Chem. Phys. **90**, 1600 (1989).
[23] D. A. V. Kliner and R. N. Zare, J. Chem. Phys. **92**, 2107 (1990).
[24] D. A. V. Kliner, K.-D. Rinnen, and R. N. Zare, Chem. Phys. Lett. **166**, 107 (1990).
[25] S. A. Buntin, C. F. Giese, and W. R. Gentry, Chem. Phys. Lett. **168**, 513 (1990).
[26] R. E. Continetti, B. A. Balko, and Y. T. Lee, J. Chem. Phys. **93**, 5719 (1990).
[27] H. Buchenau, J. P. Toennies, J. Arnold, and J. Wolfrum, Ber. Bunsenges. Phys. Chem. (in press), and references therein.
[28] G. Herzberg, *Molecular Spectra and Molecular Structure, I. Spectra of Diatomic Molecules* (Van Nostrand Reinhold, New York, 1950), p. 139.
[29] H. B. Levene, D. L. Phillips, J.-C. Nieh, D. P. Gerrity, and J. J. Valentini, Chem. Phys. Lett. **143**, 317 (1988).
[30] B. Liu, J. Chem. Phys. **58**, 1925 (1973); P. Siegbahn and B. Liu, *ibid.* **68**, 2457 (1978); D. G. Truhlar and C. J. Horowitz, *ibid.* **68**, 2466 (1978); **71**, 1514 (1978).
[31] A. J. C. Varandas, F. B. Brown, C. A. Mead, D. G. Truhlar, and N. C. Blais, J. Chem. Phys. **86**, 6258 (1987).
[32] C. W. Bauschlicher, Jr., S. R. Langhoff, and H. Partridge, Chem. Phys. Lett. **170**, 345 (1990).
[33] J. Z. H. Zhang and W. H. Miller, Chem. Phys. Lett. **159**, 130 (1989).
[34] J. G. Muga and R. D. Levine, Chem. Phys. Lett. **162**, 7 (1989).
[35] J. L. Krause and M. Shapiro, Isr. J. Chem. **29**, 427 (1989).
[36] T. Seideman, J. L. Krause, and M. Shapiro, Chem. Phys. Lett. (in press).
[37] W. J. van der Zande, R. Zhang, and R. N. Zare, *Spectral Line Shapes* (American Institute of Physics, New York, 1990), Vol. 6, pp. 301–310.
[38] Preliminary results of this study were presented at the ACS National Meeting in Boston, April, 1990.
[39] K.-D. Rinnen, D. A. V. Kliner, R. S. Blake, and R. N. Zare, Chem. Phys. Lett. **153**, 371 (1988).
[40] K.-D. Rinnen, D. A. V. Kliner, and R. N. Zare, J. Chem. Phys. **91**, 7514 (1989).
[41] K.-D. Rinnen, D. A. V. Kliner, R. S. Blake, and R. N. Zare, Rev. Sci. Instrum. **60**, 717 (1989).
[42] K.-D. Rinnen, D. A. V. Kliner, R. N. Zare, and W. M. Huo, Isr. J. Chem. **29**, 369 (1989); K.-D. Rinnen, M. A. Buntine, D. A. V. Kliner, R. N. Zare, and W. M. Huo (in preparation).
[43] C. Yu, K. B. Whaley, C. S. Hogg, and S. J. Sibener, J. Chem. Phys. **83**, 4217 (1985).
[44] D. A. McQuarrie, *Statistical Mechanics* (Harper, New York, 1976), p. 106.
[45] The BBO crystals were supplied by R. S. Feigelson and R. K. Route and grown as part of a research program sponsored in part by the Army Research Office, Contract No. DAAL03-86-K-0129, and in part by the NSF/MRL Program through the Center for Materials Research, Stanford University.
[46] R. S. Blake, Ph.D. thesis, Stanford University, Stanford, California, 1988.
[47] J. F. Ogilvie, Trans. Faraday Soc. **67**, 2205 (1971).
[48] I. Levy and M. Shapiro, J. Chem. Phys. **89**, 2900 (1988).
[49] J. J. Valentini (private communication).
[50] This conclusion does not necessarily apply to other reactions; see G. C. Schatz, D. Sokolovski, and J. N. L. Connor J. Chem. Phys. (in press).
[51] R. E. Continetti, J. Z. H. Zhang, and W. H. Miller, J. Chem. Phys. **93**, 5356 (1990).
[52] A similar conclusion has been reached for the H + *p*-H_2 reaction; see, W. H. Miller and J. Z. H. Zhang, J. Phys. Chem. (in press).
[53] S. A. Buntin, C. F. Giese, and W. R. Gentry, J. Chem. Phys. **87**, 1443 (1987).
[54] K. A. Welge, in *XII International Symposium on Molecular Beams, Abstracts of Invited Talks and Contributed Papers, May 29–June 2, 1989* (University of Perugia, Perugia), p. I.10.
[55] M. Mladenovic, M. Zhao, D. G. Truhlar, D. W. Schwenke, Y. Sun, and D. J. Kouri, Chem. Phys. Lett. **146**, 358 (1988).